

Penumbral structure and outflows in simulated sunspots

M. Rempel^{1*}, M. Schüssler², R.H. Cameron² & M. Knölker¹

¹High Altitude Observatory, NCAR, P.O. Box 3000, Boulder, Colorado 80307, USA

²Max-Planck-Institut für Sonnensystemforschung,
Max-Planck-Str. 2, 37191 Katlenburg-Lindau, Germany

*To whom correspondence should be addressed; E-mail: rempel@hao.ucar.edu.

Sunspots are concentrations of magnetic field on the visible solar surface that strongly affect the convective energy transport in their interior and surroundings. The filamentary outer regions (penumbrae) of sunspots show systematic radial outward flows along channels of nearly horizontal magnetic field. These flows were discovered 100 years ago and are present in all fully developed sunspots. Using a comprehensive numerical simulation of a sunspot pair, we show that penumbral structures with such outflows form when the average magnetic field inclination to the vertical exceeds about 45 degrees. The systematic outflows are a component of the convective flows that provide the upward energy transport and result from anisotropy introduced by the presence of the inclined magnetic field.

Sunspots are dark patches on the visible solar surface that harbor strong magnetic fields up to 4000 G (1, 2). Their central region, the umbra, is the darkest part with a brightness of about 20% of the ambient value and a largely vertically oriented magnetic field; the brighter, filamentary penumbra shows a more inclined field and a nearly horizontal plasma outflow of several $\text{km}\cdot\text{s}^{-1}$, the Evershed flow, named after its discoverer (3). While a number of simplified (and partly conflicting) models have been suggested to explain the structure and outflows of penumbrae (4), a comprehensive theoretical understanding of the basic mechanisms does not exist.

Here we present ab-initio numerical simulations of complete sunspots embedded in a realistic solar convection zone and atmosphere, including all relevant physical processes: compressible magnetohydrodynamics, partial ionization, and radiative energy transport. Previous

attempts to simulate penumbral structure in small slab-like sections of sunspots (5, 6) resulted in rather narrow penumbral regions. The generally used periodic boundary conditions at the sides of the computational box tend to suppress the extended horizontal field structures associated with sunspot penumbrae. Hence we have carried out a simulation of a pair of big sunspots (diameter 35 Mm) of opposite magnetic polarity, thereby facilitating the development of strongly inclined field between the spots. Our numerical box had a horizontal extension of 98 Mm \times 49 Mm and a depth of 6.1 Mm. The spatial grid resolution was 32 km in the horizontal directions and 16 km in the vertical. The sunspots evolved for 3.6 hours during the simulation, which was sufficient to study the penumbral structure and dynamics; processes that evolve on longer time scales such as moat flows were not fully developed in this simulation. However, the surface evolution of magnetic field shows clear indications of bipolar magnetic features transported away from the spots beyond the penumbra boundary. This is reminiscent to observations of so-called ‘moving magnetic features’ (7) (SOM, movie1.mpg: ‘Magnetogram’ movie displaying the temporal evolution of B_z on the visible solar surface, the gray scale is ranging from -3.5 kG to $+3.5$ kG). More detailed information about the physical model, the numerical code, and the simulation setup is provided in the SOM.

The simulated penumbrae show the largest extension between the sunspots of opposite polarity (Fig. 1A). The periodic horizontal boundary conditions provide three different distances: 46 Mm (middle of box) and 52 Mm in the x -direction between opposite polarity spots, and 49 Mm in the y -direction between same polarity spots. The spots show a dark umbra with some brighter umbral dots, preferentially in the weaker spot on the left. A deep magnetic structure underlies the visible penumbra, particularly so between the sunspots (Fig. 1B). A movie covering 1 hour of temporal evolution of the properties displayed in Fig. 1 (SOM, movie2.mpg) shows the inward progression of filaments in the inner penumbra.

The umbral regions have a brightness of 0.15 to 0.2 I_0 , where I_0 is the average quiet-Sun value, a Wilson depression of the visible surface by 550–600 km, and vertical field strength (B_z) up to 4 kG (Fig. 2). The quantities described here are averaged in space and time as described in the caption of Fig. 2. The penumbrae have much weaker B_z , horizontal fields (B_x) with peak values around 2 kG at the inner penumbral boundaries, and an average brightness of about 0.7 I_0 . The penumbral region exhibit systematic outflows with average horizontal velocities (v_x) of up to 6 km \cdot s $^{-1}$. The onset of these flows is closely related to the magnetic field inclination: where the average inclination with respect to the vertical exceeds 45 deg, there are systematic average outflows. With growing distance from the umbra, the outflow velocity increases and the field becomes more inclined and is nearly horizontal in the outer penumbra. These properties are consistent with observational results (1, 8).

The simulated penumbra shows strong structuring in terms of elongated narrow filaments (Fig. 3). In the inner part the magnetic field shows strong variations of the inclination between 40 deg and nearly 90 deg on scales of less than 200 km. Further out regions with strongly inclined field dominate. The velocity structure is analogous: radial outflows are concentrated in highly inclined filaments and become stronger and azimuthally more extended in the outer penumbra, where the field is almost uniformly horizontal. Vertical (up- and downward) flows

occur in narrow filaments throughout the whole penumbral region.

Analyzing the penumbral structure in vertical cuts we find that the outflows reach their peak velocities (exceeding $10 \text{ km}\cdot\text{s}^{-1}$) near the visible surface (Fig. 4). This reflects the strong height gradient of pressure and density in these layers: rising hot plasma turns over and the resulting horizontal flow is guided outward from the spot by the strong and inclined magnetic field. While the vertical field in the sunspot umbra only permits convection in the form of narrow columnar structures (9), the inclined field in the penumbra favours sheet-like upflows, which are radially extended and narrow in the azimuthal direction (6). Together with the preferred weakening of the vertical field component due to flux expulsion by the expanding rising plasma, this explains the azimuthal structuring and large azimuthal variations of the field inclination in the inner penumbra. The influence of horizontal flows on the field structure depends on the location in the penumbra. In the inner penumbra they remain rather weak and have therefore only a limited back reaction on the field structure. In the outer penumbra they become sufficiently strong to bend over field lines leading to more extended patches of horizontal field and flows. In addition to the strong localized outflows near the visible surface, there is a large-scale flow cell with plasma rising and diverging around the spot, as is evident by the general reddish color in the representation of the horizontal velocity in Fig. 4. Systematic inflows (comprising very little mass flux) are apparent in the uppermost layers of the simulation box. Because these regions are strongly affected by the upper (closed) boundary, it is not clear whether the inflows could possibly be related to the observed inverse Evershed effect in the chromosphere (10).

The central penumbral region between the spots has a mean bolometric brightness of $I_p = 0.68I_0$ (averaged over $y = \pm 3.2 \text{ Mm}$ from the midplane of the computational box and between the central vertical dotted lines indicated in Fig. 2). The mean brightness of the upflow areas is $1.1I_p$, while that of downflow areas is $0.92I_p$. The corresponding values for undisturbed granulation are $1.11I_0$ and $0.88I_0$, respectively, implying they have similar properties. However, the penumbral region shows an rms bolometric brightness contrast of 25.2%, which is substantially larger than the corresponding granulation value of 17.3%. Observations also imply a positive correlation between brightness and vertical flow direction (11). This constitutes evidence for a convective flow pattern that transports the energy flux emitted in the penumbra. Other studies show a correlation between intensity and line-of-sight velocities (12), which for sunspots observed outside the center of the solar disk is dominated by the horizontal Evershed flow. This is consistent with our findings, because in the penumbra the horizontal flow velocity is correlated with the vertical flow direction.

Our detailed analysis (SOM) shows that the spatial scales of the flows providing the major part of the convective energy transport are similar for both undisturbed granulation and penumbra. The primary difference is that there is no preferred horizontal direction for granulation, while the energy-transporting flows in the penumbra are distinctly asymmetric: convective structures are elongated in the radial direction of the sunspot. These properties were already indicated in earlier simulations (5, 6) and suggested as an explanation for the Evershed outflow in (13). The simulation shown here confirms this suggestion and demonstrates the convective nature of a fully developed penumbra.

The horizontal asymmetry of the convective flows is also manifest in the correlation of 0.42 between the corresponding flow component (v_x) and the brightness. We find that the rms of the outflowing velocity component (v_x) in the penumbra is much larger than the transverse component (v_y) (perpendicular to the filament direction), showing an asymmetry similar to that found by the scale analysis. The total rms velocity profile as a function of depth is very similar to its counterpart for undisturbed granulation, apart from a slightly higher peak value, confirming the physical similarity of convection in granulation and penumbra.

The mass flux and energy flux show similar properties with respect to the length scales and asymmetry (SOM), indicating that most of the outflowing material emerges, turns over and descends within the penumbra. In the deeper layers, there is some contribution (of the order of 10–20%) to both energy and mass flux by the large-scale flow cell surrounding the sunspots.

The analysis of our simulations clearly indicates that granulation and penumbral flows are similar with regard to energy transport; the asymmetry between the horizontal directions and the reduced overall energy flux reflect the constraints imposed on the convective motions by the presence of a strong and inclined magnetic field. The development of systematic outflows is a direct consequence of the anisotropy and the similarities between granulation and penumbral flows strongly suggest that driving the Evershed flow does not require physical processes that go beyond the combination of convection and anisotropy introduced by the magnetic field. Weaker laterally overturning flows perpendicular to the main filament direction explain the apparent twisting motions observed in some filaments (14, 15) and lead to a weakening of the magnetic field in the flow channels through flux expulsion (6).

Although our simulations of large sunspots is realistic in terms of relevant physics, it does not faithfully reproduce all aspects of the morphology of observed penumbral filaments. The penumbral regions are considerably more extended than in previous local simulations, but they are still somewhat subdued, probably owing to the proximity of the periodic boundaries. The filaments in the inner penumbrae appear to be too fragmented and short, dark lanes along bright filaments (16) form only occasionally, likely a consequence of the still limited spatial resolution of the simulation. Finally, the initial condition of the magnetic field underlying the sunspot is quite arbitrary, owing to our ignorance of the subsurface structure of sunspots. Notwithstanding these limitations, the present simulations are consistent with observations of global sunspot properties, penumbral structure, and systematic radial outflows. These and earlier simulations (5, 6, 9) suggest a unified physical explanation for umbral dots as well as inner and outer penumbrae in terms of magneto-convection in a magnetic field with varying inclination. Furthermore a consistent physical picture of all observational characteristics of sunspots and their surroundings is now emerging.

References and Notes

1. S. K. Solanki, *Astron. Astrophys. Rev.* **11**, 153 (2003).
2. J. H. Thomas, N. O. Weiss, *Ann. Rev. Astron. Astroph.* **42**, 517 (2004).

3. J. Evershed, *Mon. Not. Royal Astron. Soc.* **69**, 454 (1909).
4. J. H. Thomas, N. O. Weiss, *Sunspots and Starspots* (Cambridge University Press, 2008).
5. T. Heinemann, Å. Nordlund, G. B. Scharmer, H. C. Spruit, *ApJ* **669**, 1390 (2007).
6. M. Rempel, M. Schüssler, M. Knölker, *ApJ* **691**, 640 (2009).
7. M. Kubo, T. Shimizu, S. Tsuneta, *ApJ* **659**, 812 (2007).
8. R. Keppens, V. Martinez Pillet, *Astron. Astrophys.* **316**, 229 (1996).
9. M. Schüssler, A. Vögler, *ApJL* **641**, L73 (2006).
10. D. Dialetis, P. Mein, C. E. Alissandrakis, *Astron. Astrophys.* **147**, 93 (1985).
11. J. Sánchez Almeida, I. Márquez, J. A. Bonet, I. Domínguez Cerdeña, *ApJ* **658**, 1357 (2007).
12. L. R. Bellot Rubio, R. Schlichenmaier, A. Tritschler, *Astron. Astrophys.* **453**, 1117 (2006).
13. G. B. Scharmer, Å. Nordlund, T. Heinemann, *ApJL* **677**, L149 (2008).
14. K. Ichimoto, *et al.*, *Science* **318**, 1597 (2007).
15. V. Zakharov, J. Hirzberger, T. Riethmüller, S. Solanki, Kobel, P., *Astron. Astrophys.* **488**, L17 (2008).
16. G. B. Scharmer, B. V. Gudiksen, D. Kiselman, M. G. Löfdahl, L. H. M. Rouppe van der Voort, *Nature* **420**, 151 (2002).
17. High-performance computing resources were provided by NCAR's Computational and Information Systems Laboratory. The National Center for Atmospheric Research is sponsored by the National Science Foundation.

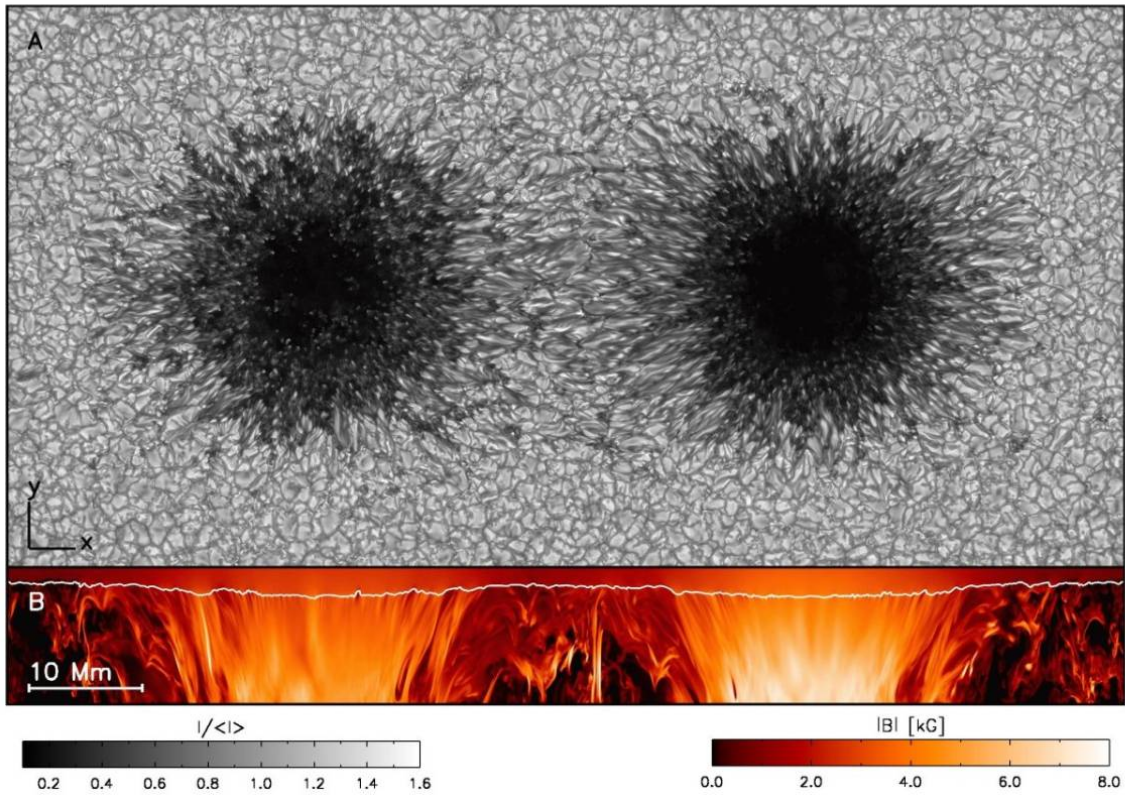


Figure 1: Snapshot from the simulation. **(A)** Surface brightness map of the sunspot pair and the surrounding convective pattern (granulation). **(B)** Color representation of the field strength (saturated at 8 kG) in a vertical cut through the midplane of the simulation box at $y = 25$ Mm. The vertical direction is stretched by a factor of 2. The white line indicates the height level of the visible surface (optical depth unity).

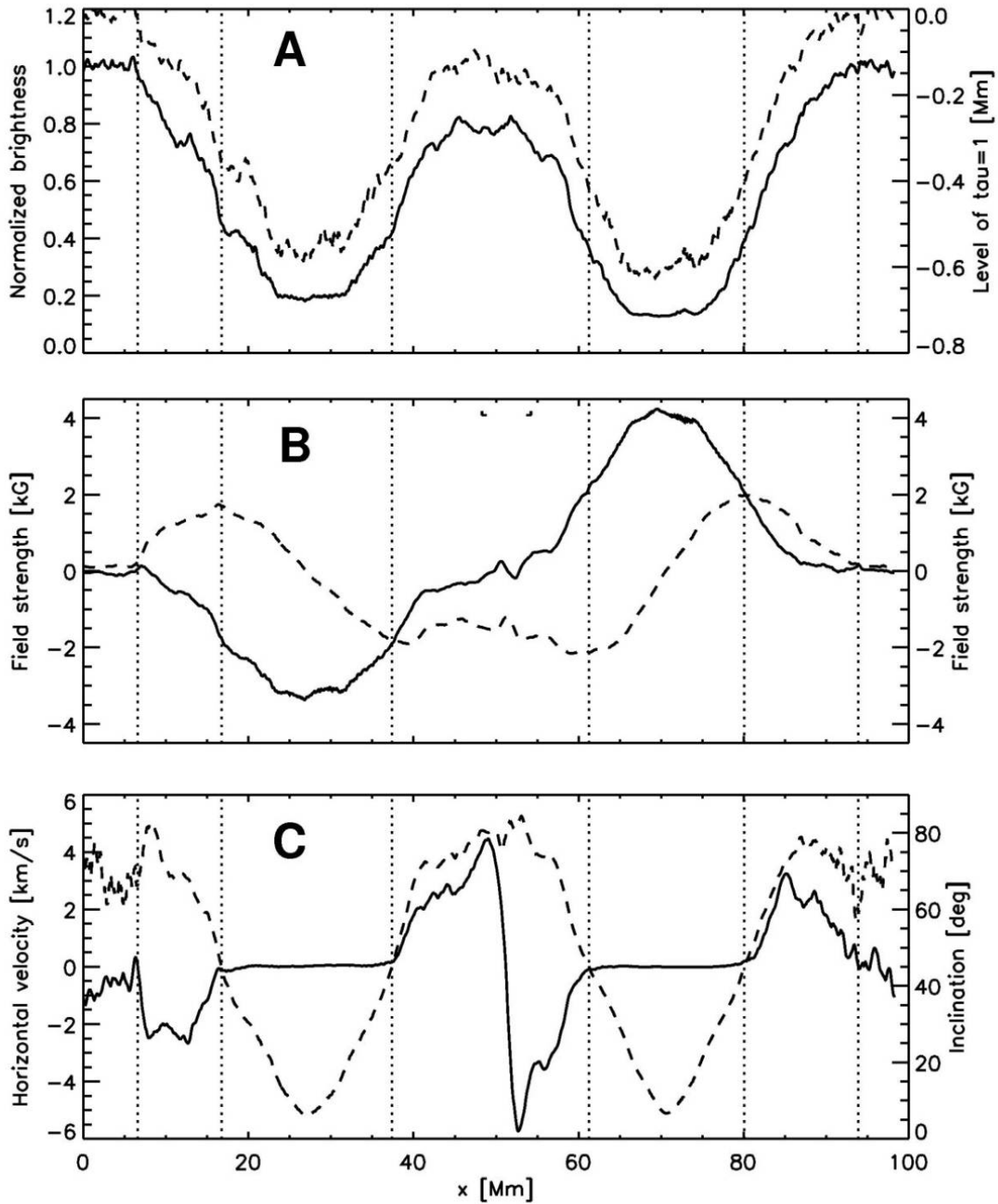


Figure 2: Horizontal profiles of various quantities at the visible surface, averaged over ± 3.2 Mm from the midplane in y and time-averaged over one hour. (A) Brightness (normalized to the average over non-magnetic regions, solid) and depression of the visible surface with respect to non-magnetic regions (Wilson depression, dashed). (B) Strength of the vertical (B_z , solid) and horizontal (B_x , dashed) magnetic field components. (C) Horizontal velocity (v_x , solid) and magnetic field inclination with respect to the vertical (dashed). Vertical dotted lines indicate the regions with systematic penumbral outflows.

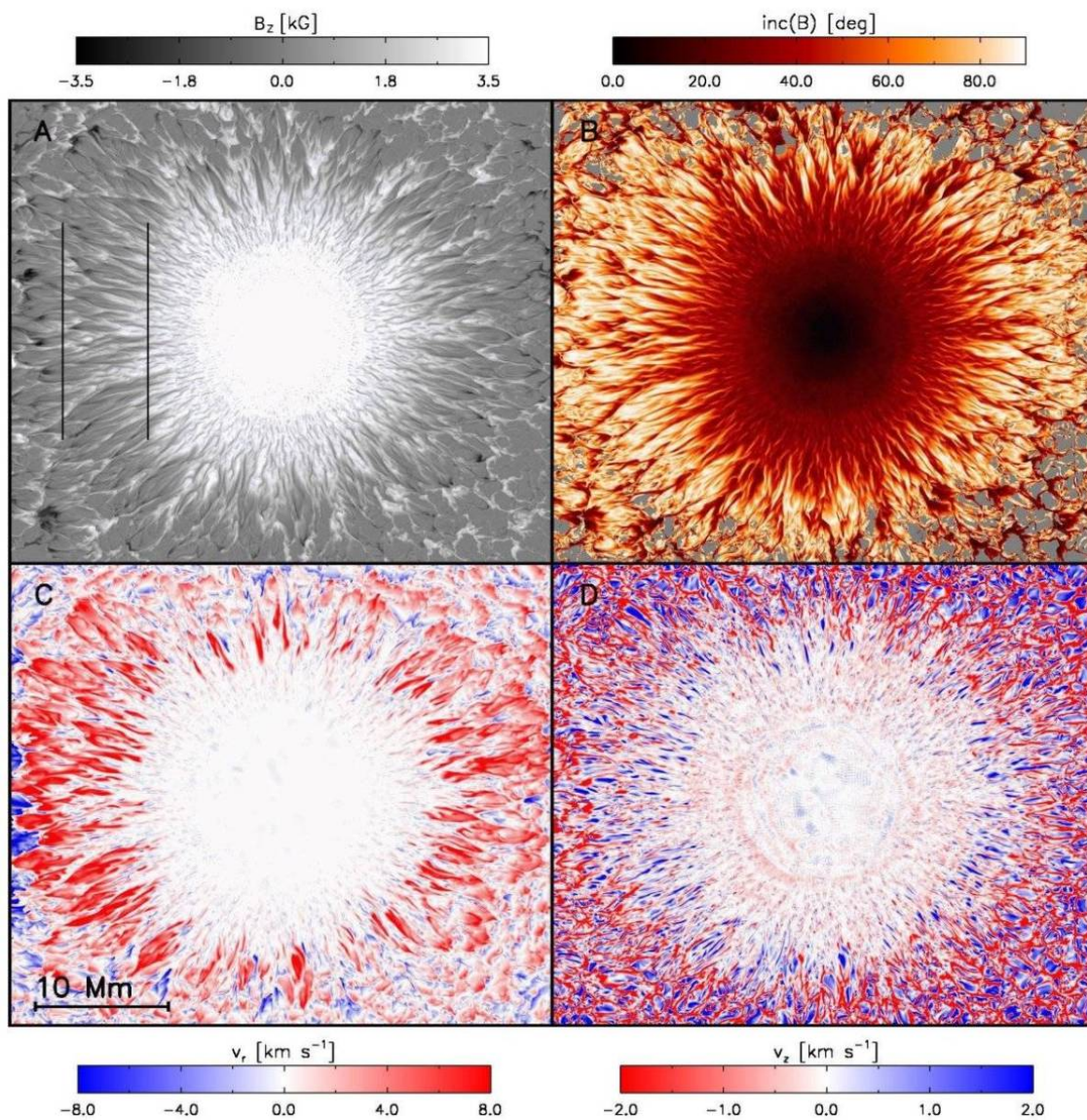


Figure 3: Magnetic field and velocity structure at the visible surface for the sunspot on the right side of Fig. 1. **(A)** Vertical field component (saturated at ± 3.5 kG). **(B)** Inclination angle of the magnetic field with respect to the vertical direction (grey indicates $|B| < 200$ G). **(C)** Radial outflow velocity (saturated at ± 8 km \cdot s $^{-1}$, red indicates outflows). **(D)** Vertical velocity (saturated at ± 2 km \cdot s $^{-1}$, red indicates downflows). The vertical lines in A indicate the positions of the cuts shown in Fig. 4.

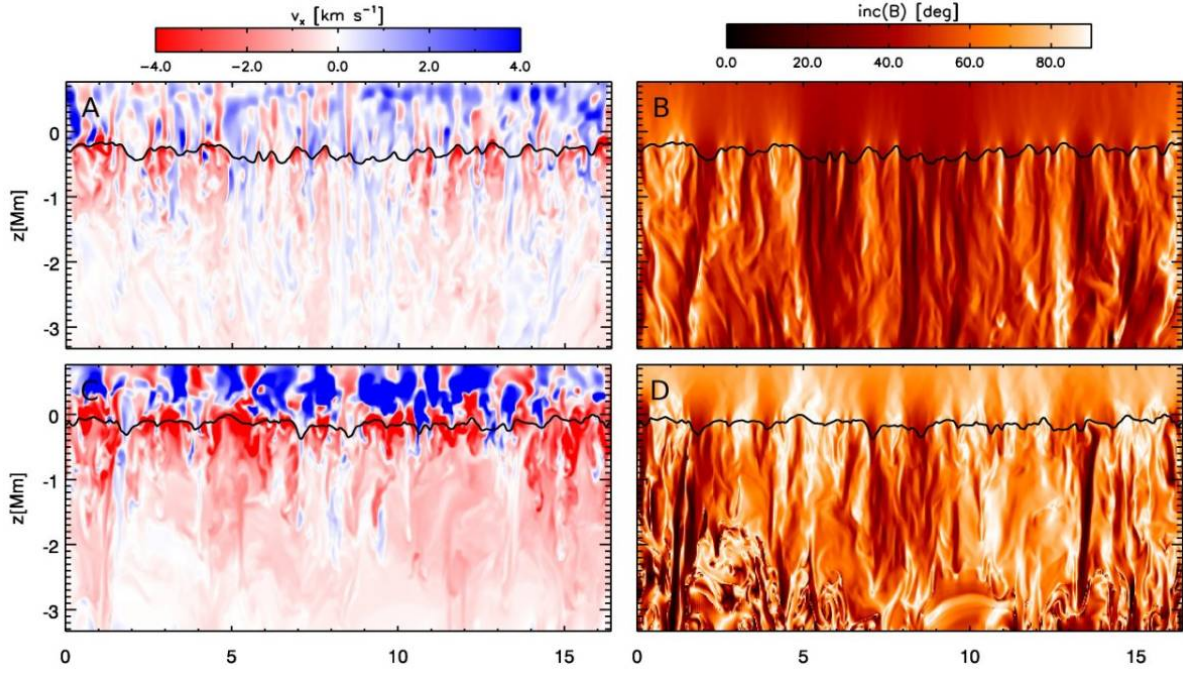


Figure 4: Vertical cuts through the penumbra (indicated by the black lines in Fig. 3A). The vertical direction is stretched by a factor of 2. Shown are the horizontal velocity component v_x (left) and the field inclination (right). (A, B) Inner penumbra (right line in Fig. 3A). (C, D) Outer penumbra (left line in Fig. 3A). The color representation of v_x is saturated at $\pm 4 \text{ km}\cdot\text{s}^{-1}$. Black lines indicate the visible surface (optical depth unity).

Appendix: Supporting online material (SOM)

1 Simulation setup

The simulation presented here has been carried out with the *MURaM* MHD code (1, 2), with modifications described in (3). The physics, numerics and boundary conditions are similar to earlier runs described there, the primary difference here is the far larger domain size and the initial magnetic field configuration.

It is currently still out of reach to run an ab-initio simulation of the formation of an active region, primarily due to the large vertical extent of the simulation domain required for this purpose. In this study we focus on a 6.1 Mm deep domain to study the near-surface structure of a pair of opposite polarity sunspots. We start with a $98 \times 49 \times 6.1$ Mm domain of thermally relaxed convection, in which the $\tau = 1$ surface is located about 700 km beneath the top boundary. The magnetic field is initialized as a pair of axisymmetric opposite-polarity sunspots, which are based on the self-similar field configuration used by (4). Each spot comprises about $1.6 \cdot 10^{22}$ Mx magnetic flux, but their initial field strength is different (5 kG and 7 kG, respectively, at the bottom of the domain, dropping to about 3 kG in the near photospheric layers). In the course of the simulation, this leads to a pair of sunspots with a photospheric field strength of about 3.2 kG (spot on the left) and 4.2 kG (spot on the right). The separation of the two spots in the middle of the domain is 46 Mm, about 3 Mm less than half of the horizontal extent in the x -direction. Owing to the periodic horizontal boundary condition this setup allows to study a variety of different combinations of field strength and inclination angles: In the x -direction we have opposite polarity spots with 3.2 and 4.2 kG strength and separations of 46 and 52 Mm in between, in the y -direction the magnetic field is less inclined since periodicity imposes same polarity spots in a distance of 49 Mm. As a consequence we can study several realizations of penumbra in one simulation run and evaluate the robustness of our results.

We ran the simulation for the first hour of simulated time with a rather low numerical grid resolution of $96 \times 96 \times 32$ km to get past initial transients. The second hour was performed at a medium resolution of $48 \times 48 \times 24$ km and then followed by another 1.6 hours with a resolution of $32 \times 32 \times 16$ km (corresponding to $3072 \times 1536 \times 384$ grid cells). The results presented here are based on snapshots near the end of the high-resolution run and partly on temporal averages over the last hour. The total duration of the run of about 3.6 hours is still very short compared to the typical lifetime of a sunspot, so that the umbral regions are not yet completely thermally relaxed. However, the dynamical time scales for the penumbral regions is much shorter and no significant change or trend of the properties discussed here has been observed over the 1.6 hours duration of the high resolution run.

2 Scales and anisotropy of energy and mass flux

2.1 Energy flux

The vertical energy flux is given by

$$F_z(x, y, z) = \rho v_z \left(\varepsilon + \frac{p}{\rho} + \frac{1}{2}v^2 \right) + F_z^M \quad (1)$$

Here ε denotes the specific internal energy and F_z^M the vertical component of the Poynting flux. In the following discussion we ignore the Poynting flux, which does not exceed a few percent of the total energy flux.

To quantify the scale dependence as well as possible anisotropies we consider here a dimensionless measure for the decorrelation of the energy flux when mass flux and specific enthalpy are smoothed independently over a certain length scale L . We define here dimensionless functions of the height z and smoothing length L that quantify the decorrelation of the energy flux for smoothing in the x -direction, P_x , and in y -direction, P_y :

$$\begin{aligned} P_x(z, L) &= \frac{\int \langle F_z \rangle_L^x dx dy}{\int F_z dx dy} \\ P_y(z, L) &= \frac{\int \langle F_z \rangle_L^y dx dy}{\int F_z dx dy} . \end{aligned} \quad (2)$$

Here the quantity $\langle F_z \rangle_L^x$ (and equivalent $\langle F_z \rangle_L^y$) is given by

$$\langle F_z \rangle_L^x(x, y, z) = \langle \rho v_z \rangle_L^x \left\langle \varepsilon + \frac{p}{\rho} + \frac{1}{2}v^2 \right\rangle_L^x . \quad (3)$$

The brackets indicate smoothed quantities (to remove the contributions of scales smaller than L), which are defined through a convolution using a Gaussian G_L with the length scale L as full width at half maximum. For example, a 1-dimensional smoothing in the x -direction is defined as

$$\langle f \rangle_L^x(x, y, z) = \int f(x', y, z) \cdot G_L(x - x') dx' . \quad (4)$$

Smoothing vertical mass flux and the specific enthalpy guarantees a balanced mass flux at each scale L , provided that the original mass flux was balanced within the domain. In general the vertical mass flux is not necessarily balanced within a subdomain, owing to the presence of vertical oscillations and, possibly, of flows on scales larger than the subdomain. A meaningful determination of the convective energy flux requires that these contributions must be eliminated. We achieve this by subtracting, at each height level, the density-weighted vertical mean velocity $\bar{v}_z(z) = \int \rho v_z dx dy / \int \rho dx dy$ from the vertical velocity component before energy and mass fluxes are computed. As a consequence, we include only the contribution from motions that overturn within the subdomain boundaries.

2.2 Mass flux

We also apply the same method to analyze the scale dependence and anisotropy of the mass flux. To this end we smooth ρv_z as described above and compute the quantities Q_x and Q_y in the following way:

$$\begin{aligned} Q_x(z, L) &= \frac{\int |\langle \rho v_z \rangle_L^x| dx dy}{\int |\rho v_z| dx dy} \\ Q_y(z, L) &= \frac{\int |\langle \rho v_z \rangle_L^y| dx dy}{\int |\rho v_z| dx dy} \end{aligned} \quad (5)$$

Since the mass flux is balanced, i.e. $\int \rho v_z dx dy = 0$, we consider here the absolute value. Our analysis will therefore provide the typical scale on which most of the mass flux turns around.

2.3 Results

To compare the properties of the energy flux in a penumbral region and almost undisturbed granulation we apply this procedure to two subdomains indicated in Fig. 5. Both regions have about 32×16 Mm horizontal extent (note that both boxes are contiguous owing to the periodic boundary condition). Fig. 6 presents the scale dependence and anisotropy of the energy flux comparing the granulation and penumbral region. Panel a) shows the geometric average of P_x and P_y for granulation. Different height levels are color-coded, with depth increasing from blue toward red. The uppermost height level corresponds to the position at which the average pressure scale height is 200 km, the distance between the height levels is 320 km. The total range covered in the vertical direction is about 4.8 Mm, excluding the lower most 500 km that are affected by the boundary condition. With increasing smoothing length scale L (thus eliminating the contribution from small scales) the remaining convective energy flux decreases and drops by a factor of about 2 when L reaches a value of about 400 km in the near photospheric layers. For the deeper layers the corresponding curves are shifted toward larger values of L (approximately $L \sim H_p$). The anisotropy, defined as P_y/P_x , (not shown here) is very close to 1 with fluctuations of up to 20% on larger scales. Panels b) and c) present the results from applying the same procedure to the penumbral region between the two spots as indicated by the central white box in Fig. 5. While the overall shape of the curves remains the same, some distinct differences occur for P_x and P_y . In the case of P_x , the depth dependence is strongly reduced and all curves almost coincide with a curve corresponding to that from about 2 – 3 Mm depth in the case of granulation. On the other hand the depth dependence of P_y is similar to that of granulation, but overall the scales are reduced by a factor of about 2. Panel d) shows the anisotropy defined through the ratio P_y/P_x . For scales of less than about 2000 km, the deep layers remain close to isotropic, while the anisotropy reaches values of about 0.25 in the near photospheric layers. According to our definition of the anisotropy values < 1 indicate smaller scales in the y as compared to the x -direction (i.e. the quantity $\int \langle F_z \rangle_L^y dx dy$ falls off quicker than $\int \langle F_z \rangle_L^x dx dy$ with increasing L). For scales larger than 2000 km the deeper

layers have anisotropies > 1 , indicating a contribution from large scale flows more coherent in the y direction. In the deep layers contributions from large scales in P_y remain at about 20% compared to about 10% in undisturbed granulation. The difference of 10% can be attributed to the presence of the large scale Evershed/moat flow system in the penumbra region.

On a qualitative level the behavior of the mass flux (Fig. 7) is not distinctly different from that of the energy flux. Overall the typical scale for the overturning of mass is larger than the typical scale for the energy transport in both granulation and penumbra. The degree of anisotropy of the mass flux is reduced compared to the anisotropy of the energy flux. The increase of anisotropy on larger scales is more pronounced on all height levels. In the deep layers the Evershed/moat flow contribution to the mass flux is about 10% to 15% (values of Q_y remain around 45% as compared to 30% in the case of granulation).

While the penumbral region shows distinct differences from granulation in terms of anisotropy in height levels extending several Mm downward, we find no significant change in the relative contribution of large and small scales in the overall energy transport. The presence of large scale contributions is more prominent in the mass flux, but not substantially enlarged compared to granulation.

The similarities between energy and mass transport in granulation and penumbra are also evident from the height dependence of rms velocities (Fig. 8). The computation of the rms velocities in the penumbra is based on a smaller subdomain of half the size as indicated in Fig. 5 to exclude umbral regions which would lower the overall rms velocity (for computing the rms velocities a balanced mass flux within the subdomain is less important). We present in panels a) and b) v_{rms} (black) $v_{x \text{ rms}}$ (red), $v_{y \text{ rms}}$ (blue) and $v_{z \text{ rms}}$ (green) for granulation and penumbra, respectively; panels c) and d) display the rms velocities normalized by the total rms. A comparison for the profile of v_{rms} between granulation and penumbra does not reveal a significant difference, except for slightly larger velocities in the photosphere and a steeper increase toward the photosphere. In the case of granulation vertical motions contribute about 50% to the kinetic energy, while both horizontal components contributing about 25%. These contributions are almost independent of depth except near the bottom where v_z is preferred over horizontal motions due to the boundary condition. In the case of the penumbra the kinetic energy is dominated by the component in the direction of filaments (x) which contributes about 55%, the contribution of vertical motions is reduced to about 35% while horizontal motions perpendicular to filaments contribute only about 10% in the near photospheric layers.

Overall we do not see a strong indication for a fundamental difference between energy and mass transport in granulation and penumbra, except for the anisotropy introduced by the presence of strong horizontal magnetic field. Scales in the direction of the horizontal field become less dependent on the pressure scale height, while scales perpendicular to the preferred field direction remain strongly dependent on pressure scale height and are reduced. As a consequence energy and mass transport become more anisotropic toward the surface. The anisotropy leads to a reduction of horizontal motions perpendicular to the field direction, while the component parallel to the field is increased. The total rms velocity does not show a significant change, indicating that the kinetic energy of convective motions remains similar, it is just differently

distributed among the x , y and z direction. These similarities strongly indicate that driving the Evershed flow does not require physical processes that go beyond the combination of convection and anisotropy introduced by the magnetic field.

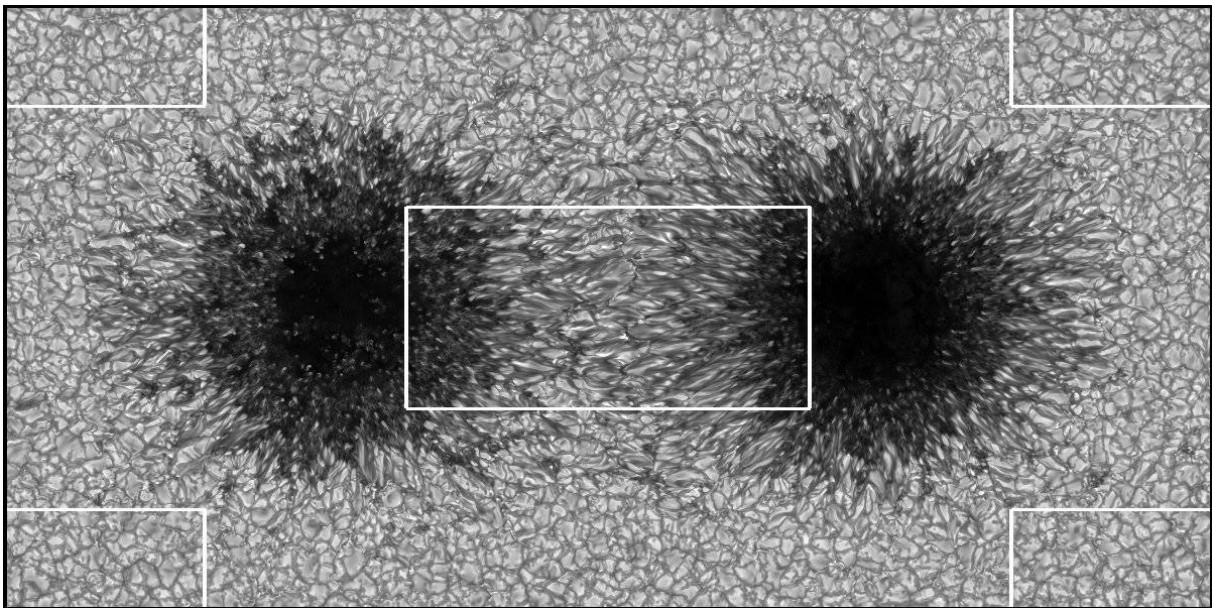


Figure 5: White boxes indicate the domains for which we compare the properties of energy and mass flux. The central box encloses most of the penumbral region between both spots, the box near the corners encloses a region of equal size with almost undisturbed granulation.

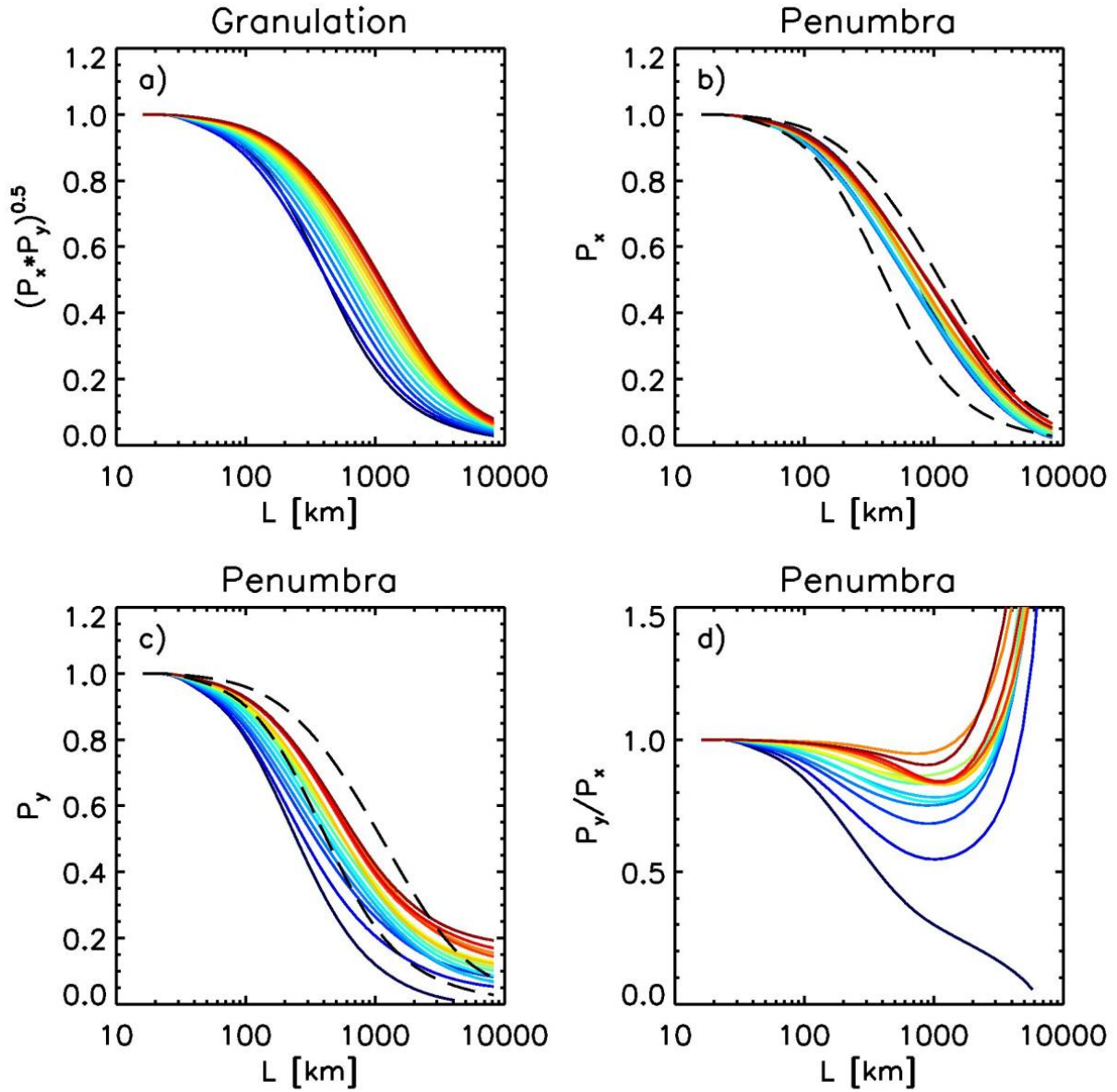


Figure 6: Scale dependence and anisotropy of energy flux in solar granulation and penumbral region. Panel a) shows undisturbed granulation for reference. Different height levels are color-coded ranging from the photosphere (dark blue) to the bottom of the domain (dark red), spanning a total of 4.8 Mm. The black dashed lines in panels b) and c) correspond to the dark blue (near photosphere) and dark red (near bottom of domain) curves in panel a). Panels b) and c) display the corresponding quantities for the penumbral region, panel d) the derived anisotropy of the energy flux with respect to the x and y direction.

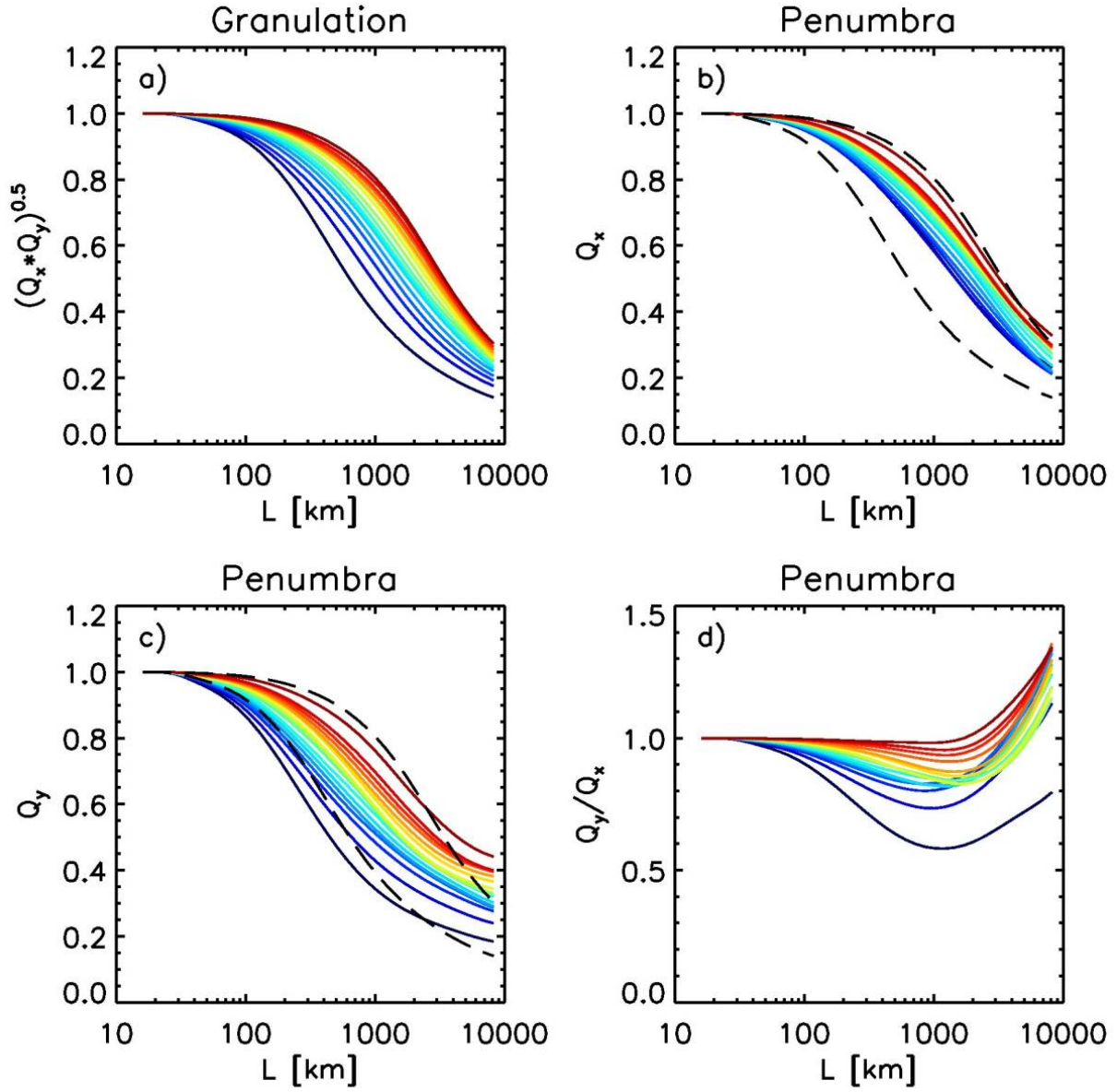


Figure 7: Same as Fig. 7 for the mass flux as defined by Eq. (5).

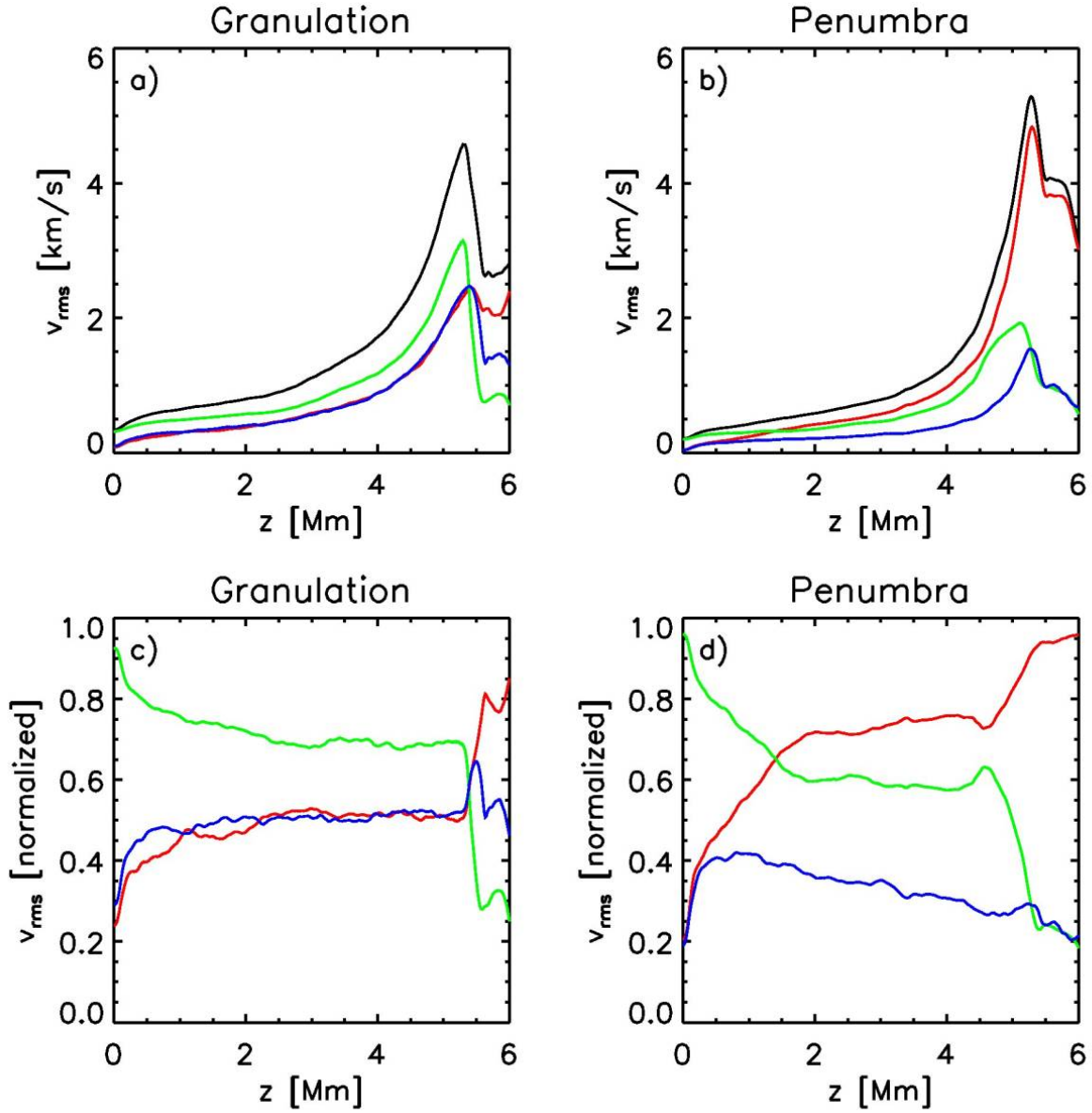


Figure 8: Comparison of rms velocities in granulation and penumbra. Panels a) and b) show v_{rms} (black) $v_{x,rms}$ (red), $v_{y,rms}$ (blue) and $v_{z,rms}$ (green) for granulation and penumbra, respectively. Panels c) and d) present $v_{x,rms}$, $v_{y,rms}$ and $v_{z,rms}$ normalized by v_{rms} .

References and Notes

1. A. Vögler, Three-dimensional simulations of magneto-convection in the solar photosphere, Ph.D. thesis, University of Göttingen, Germany, <http://webdoc.sub.gwdg.de/diss/2004/voegler> (2003).
2. A. Vögler, *et al.*, *Astron. Astrophys.* **429**, 335 (2005).
3. M. Rempel, M. Schüssler, M. Knölker, *ApJ* **691**, 640 (2009).
4. M. Schüssler, M. Rempel, *Astron. Astrophys.* **441**, 337 (2005).